Check for updates

View Article Online
View Journal

Nanoscale Advances

Accepted Manuscript

This article can be cited before page numbers have been issued, to do this please use: Z. Sun, Y. Wang, P. R. Bianco and Y. Lyubchenko, *Nanoscale Adv.*, 2020, DOI: 10.1039/C9NA00712A.

This is an Accepted Manuscript, which has been through the Royal Society of Chemistry peer review process and has been accepted for publication.

Accepted Manuscripts are published online shortly after acceptance, before technical editing, formatting and proof reading. Using this free service, authors can make their results available to the community, in citable form, before we publish the edited article. We will replace this Accepted Manuscript with the edited and formatted Advance Article as soon as it is available.

You can find more information about Accepted Manuscripts in the Information for Authors.

Please note that technical editing may introduce minor changes to the text and/or graphics, which may alter content. The journal's standard Terms & Conditions and the Ethical guidelines still apply. In no event shall the Royal Society of Chemistry be held responsible for any errors or omissions in this Accepted Manuscript or any consequences arising from the use of any information it contains.

ROYAL SOCIETY OF CHEMISTRY

rsc.li/nanoscale-advances

Please do not adjust margins

View Article Online
DOI: 10.1039/C9NA00712A

ARTICLE

Nanoscale interaction of RecG with mobile fork DNA

Received 00th January 20xx,
Accepted 00th January 20xx

DOI: 10.1039/x0xx00000x

Zhiqiang Sun[a], Yaqing Wang[a], Piero R. Bianco[b*], and Yuri L. Lyubchenko[a*]

The RecG DNA helicase is a guardian of the bacterial genome where it dominates stalled DNA replication fork rescue. The single-stranded DNA binding protein (SSB) is involved in this process and promotes the binding of RecG to stalled replication forks. Atomic force microscopy (AFM) was used to investigate the interaction of RecG and SSB on a mobile fork substrate capable of being regressed. In the absence of proteins, the fork undergoes spontaneous dynamics between two states defined by the length of the DNA complementarity at the fork. Binding of SSB does not affect these dynamics as it binds to single-stranded regions as expected. In contrast, RecG interacts with the two states quite differently. We demonstrate that RecG has two modes of interaction with fork DNA in the presence of SSB and ATP. In the first mode, RecG translocates over the duplex region and this activity is defined by SSB-mediated remodeling of the helicase. In the second mode, RecG utilizes its helicase activity to regress the fork, in an ATP-dependent manner, displacing SSB on the ssDNA. Overall, our results highlight two functions of RecG that can be employed in the regulation of stalled DNA replication fork rescue.

Introduction

The inherently accurate and highly processive process of duplication of the genome depends on a firm reliance on the cooperation between the homologous recombination and DNA repair machinery. [1-3] The replication machinery can be disrupted due to frequently encountered roadblocks that have the potential to stall or collapse a replication fork. In this case, the importance of interplay arises. Once forks stall, the action of the recombination machinery is needed for fork rescue. RecG catalyzes fork regression which results in movement of the fork in a net backward direction away from the DNA impediment resulting in the formation of a Holliday junction (HJ). RuvAB binds to the HJ, resulting in additional processing, ultimately resulting in the resurrection of the fork [4-7].

For regression to occur, RecG forms an intimate complex with the fork [8]. Here, the wedge domain of the helicase binds to the fork in the DNA while the helicase domains are predicted to bind to the parental duplex region ahead of the fork. Modeling of RecG revealed that the enzyme unwinds the replication fork through a structural transition with the helicase domains by hydrolyzing ATP [9].

In addition to RecG, SSB plays an essential function in fork rescue by enhancing and controlling the activity of RecG in the early stages of the reaction [6, 7, 10-12]. We have recently utilized static fork substrates and atomic force microscopy (AFM) to understand how these proteins function at a fork. We demonstrated that the interaction of fork-bound SSB leads to remodeling of RecG during the loading process onto the DNA. As a result, RecG becomes capable of spontaneous translocation ahead of the replication fork over distances as large as 200 bp and this was directly visualized by time-lapse, high-speed AFM [13, 14]. As the forks used in this study were static, fork regression could not be visualized and in addition, the interplay between SSB and RecG during this process could not be studied.

Therefore, to characterize fork transactions at conditions allowing for the fork mobility we constructed a mobile fork substrate containing a 41 bp complementarity between the single-stranded tail (leading strand arm of the fork) and the lagging strand which is duplex DNA (Figure 1). Due to the design of the fork, it was anticipated that it would interconvert between two states, S1, and S2, driven by spontaneous branch migration. As expected, in the absence of proteins, these two states were directly observed using AFM. Furthermore, in the presence of SSB, a bimodal distribution of the protein position corresponding to two states of the fork was observed. In the absence of ATP, RecG bound preferentially to one state (state S1), while in the presence of ATP, RecG regressed the fork and displaced SSB in the process. SSB maintains the fork structure (state S2) following regression by RecG. These findings show that the DNA helicase couples DNA unwinding to duplex rewinding and the displacement of proteins bound to the DNA, consistent with a previous single-molecule study [5].

Methods

[a] Department of Pharmaceutical Sciences, University of Nebraska Medical Center, Omaha, NE 68198-6025, USA Email: ylyubchenko@unmc.edu
[b] Center for Single Molecule Biophysics and Department of Microbiology and Immunology, University at Buffalo, SUNY, Buffalo, NY 14214, USA. Email: pbianco@buffalo.edu

Electronic Supplementary Information (ESI) available: [details of any supplementary information available should be included here]. See DOI: 10.1039/x0xx00000x

Open Access Article. Published on 11 February 2020. Downloaded on 2/21/2020 10:39:26 AM.
This article is licensed under a Creative Commons Attribution 3.0 Unported Licence.

Nanoscale Advances Accepted Manuscript

Please do not adjust margins

View Article Online DOI: 10.1039/D0NA00713A

Open Access Article. Published on 11 February 2020. Downloaded on 2/21/2020 10:39:26 AM. This article is licensed under a Creative Commons Attribution 3.0 Unported Licence.

Protein preparations.

RecG protein was purified as described previously[7]. Briefly, the protein was eluted using a linear gradient (10–1000 mM NaCl) with RecG eluting between 250 and 360 mM NaCl on a 100 ml Q-Sepharose column equilibrated in buffer A [20 mM Tris-HCl (pH 8.5), 1 mM EDTA, 1 mM DTT, 10 mM NaCl]. The pooled fractions were then subjected to heparin FF and hydroxylapatite chromatography. Pooled fractions from the hydroxylapatite column were dialyzed overnight in S buffer [10 mM KPO4 (pH 6.8), 1 mM DTT, 1 mM EDTA and 100 mM KCl]. The protein was applied to a 1 ml MonoS column and eluted using a linear KCl gradient (100–700 mM) with RecG eluting at 350 mM KCl. The fractions containing RecG were pooled and dialyzed overnight against storage buffer [20 mM Tris-HCl (pH 7.5), 1 mM EDTA, 1 mM DTT, 100 mM NaCl and 50% (v/v) glycerol]. The protein concentration was spectrophotometrically determined using an extinction coefficient of 49500 M^{-1} cm^{-1}[15].

SSB protein was purified from strain K12DH1Dtrp, as described in ref [16]. The concentration of purified SSB protein was determined at 280 nm using e = 30, 000 M^{-1} cm^{-1}. The site size of SSB protein was determined to be 10 nucleotides per monomer by monitoring the quenching of the intrinsic fluorescence of SSB that occurred on binding to ssDNA, as described earlier [17, 18].

Preparation of fork substrate F12.

The substrate was assembled from two duplexes and the core fork segment, similar to our previous methodology[13]. Briefly, the constructs of the two duplexes were precisely the same as the one we used previously[13, 14]. To assemble the core fork segment, four types of the ssDNA oligos (O30, O45, O46, O47) were mixed with the same molar ratio and annealed by heating to 95°C. The sequences of the Oligos were shown in Table 1. The two duplexes and the core fork segment were ligated together in ratio 1:1:1 overnight at 16°C. The final products were purified with HPLC using a TSKgel DNA-STAT column. All oligonucleotides were bought from IDT (Integrated DNA Technologies, Inc. Coralville, Iowa, USA).

Preparation of DNA-protein complexes.

SSB-DNA complexes. DNA (final concentration: 20nM) was mixed with the SSB tetramer in a molar ratio of 1:2, and incubated in 10µl of binding buffer [10mM Tris-HCl (pH 7.5), 50 mM NaCl, 5 mM MgCl2, 1 mM DTT] for 10 min.

RecG-DNA complexes. DNA (final 20nM) was mixed with RecG in a molar ratio of 1:4, and incubated in 10µl of binding buffer for 10 min.

SSB-RecG-DNA complexes. SSB tetramer (final 20nM) and RecG were premixed in the molar ratio 1:2 in 30µl of binding buffer on ice for 30min. DNA was mixed with the SSB-RecG complexes in a molar ratio of 1:2, and incubated in 10µl of binding buffer for 30 min. The final molar ratio of DNA:SSB: RecG was 1:2:4.

AFM imaging and data analysis.

Imaging. 1-(3-aminopropyl) silatrane (APS) functionalized mica was used as the AFM substrate for all experiments. Briefly, freshly cleaved mica was incubated in 4ml APS (167 µM) in a cuvette for 30 min and then rinsed with ddH2O thoroughly, as described in ref [14]. Ten microliters of the sample were deposited onto the APS mica for 2 min, cleaned with ddH2O, and dried with a gentle Argon gas flow. Images were acquired using tapping mode in the air on a MultiMode 8, Nanoscope V system (Bruker, Santa Barbara, CA) using TESPA probes (320 kHz nominal frequency and a 42 N/m spring constant) from the same vendor.

Table 1 The sequence of different oligos.

Oligo name	Sequence
O30	TCATCTGCGTATTGGGCGCTCTTCCGCTTCCTATCT
O45	TCGTTCGGCTGCGGCGAGCGGGATCTAGTAGCTCTG CAGCACTGCATAATTATCAGCTCACTCATA
O46	GCTTATGAGTGAGCTGATAATTATGCAGTGCTGCAG AGCTACTAGATCGCCGCTCGCCGCAGCCGAACGACC TTGCGCAGCGAGTCAGTGAGATAGGAAGCGGAAGA GCGCCCAATACGCAGA
O47	CACTGACTCGCTGCGCAAGGTCGTTCGGCTGCGGCG AGCGGCGATCTAGTAGCTCTGCAGCCTTCATCTTTG GGTTCACTTTCTCCAC

Data analysis.

The dry sample AFM images were analyzed using the FemtoScan Online software package (Advanced Technologies Center, Moscow, Russia). The positions of SSB were measured from the end of the short arm on the DNA substrate to the center of the protein. The contour lengths of the DNA were then measured from the protein to the other end of DNA. The yield of protein-DNA complexes was calculated from the ratio of compounds to the total number of DNA molecules.

Sample preparation for time-lapse imaging in liquid with high-speed AFM (HS-AFM).

The fresh cleaved mica was incubated with 2.5µl of the APS for 30min and then washed with ddH_2O. The DNA samples (2.5 µl) were then deposited onto the APS mica and incubated for 2 min. The sample was then rinsed with 20µl of the binding buffer. Time-lapse images were acquired using a commercial HS-AFM instrument (RIBM Co. Ltd., Tsukuba, Japan) using custom-built, high-aspect ratio, high-frequency carbon probes (based on BL-AC10DS, Olympus Corp., Tokyo, Japan). The image size was usually set to 300x300 nm with 1nm/pixel resolution, and the scan rate was 800 ms/frame.

Results

Experimental design.

The fork design used in this study has a 3'-end, 69nt ssDNA tail inserted between two heterologous duplex regions of different lengths (Figure 1), similar to the static fork DNA substrate Fork 4 (F4) which we used previously [13]. We name the new construct Fork 12 (F12). The left duplex region corresponds to parental DNA; the single strand tail is the leading strand arm, while the

Nanoscale Advances Accepted Manuscript

 This journal is © The Royal Society of Chemistry 20xx

View Article Online
DOI: 10.1039/C9NA00713A

right duplex region corresponds to the lagging strand arm of the fork. In contrast to the F4 design, the central core of the F12 substrate is homologous as there is a 41nt region of ssDNA from the fork position which is complementary to the template lagging strand. This design allows the joint position to move between state S1 and state S2 as shown in Figure 1. In state S1, the length of the parental duplex (short duplex fragment) is 280bp, and the lagging duplex length is 423bp, while the ssDNA region is 69nt. In state S2, the length of parental duplex (short duplex fragment) is 321bp and the lagging duplex length is 382bp, in which case part of the ssDNA (28nt) anneals to parental strand and the other part (41nt) anneals to the lagging strand. This dynamic design is predicted to allow the fork to move between two states and more importantly, permit the study of the fork regression process.

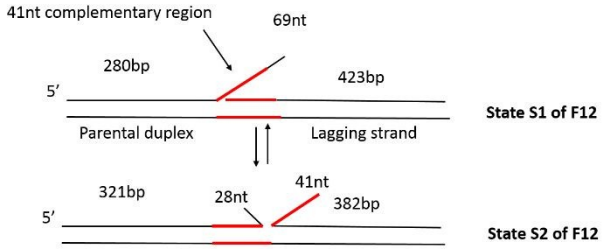

Figure 1. Dynamic fork design to study fork rescue process. The fork substrate (F12) is comprised of a 3'-end 69nt ssDNA flanked by duplex regions of different lengths. Within the 69nt ssDNA, there is a 41nt region (colored red), complementary to the lagging strand arm of the fork. Consequently, the fork can equilibrate between two states designated S1 and S2. Interconversion between S1 and S2 involves the formation of duplex DNA between the 41nt ssDNA and the complement in the lagging strand arm of the fork. This results in a net movement of the fork by 41 bp, from the left to the right in the molecules as shown, concomitant with an increase in the length of the parental duplex and a decrease in the length of the lagging strand arm.

The dynamics of F12 between the two states.

To determine whether our design does, in fact, allow fork migration between the two states, we imaged the substrate using AFM. A representative frame of AFM images of F12 on APS mica is shown in Figure 2. We found some F12 DNA molecules have sharp kinks as shown in the zoomed-in images (indicated with arrows). The kink can be explained by the nick at the fork joint. The long ssDNA at the fork position can also contribute to the kink formation. This interpretation is supported by mapping of the kink position by measuring the distance from the end of the parental duplex to the kink position. The distribution of fork positions and the full length of DNA are shown in Figure 2B and C. The histogram of fork positions can be approximated by a bimodal Gaussian distribution. The average peak positions are 281 ± 9 bp and 308 ± 12 bp which corresponds to the two states of F12. This result means the fork is dynamic and can move between two states as designed.

The full length of F12 distribution is shown in Figure 2C and it is approximated with a single peak Gaussian. The peak position is 700 ± 27 bp which corresponds to the length of F12 (703 bp). A similar analysis was applied to the immobile fork DNA substrate (F4), which has no complementarity with the ssDNA segment and the data are shown in Supplementary Figure S1. There is only one peak on the fork position distribution with the peak position 271 ± 16 bp, which is in line with the fork position (280 bp)[13].

Assembly of a Holliday junction within the F12 template.

To further confirm the mobility of fork position between the two states, a 69 nt ssDNA, which is complementary to the 69 nt ssDNA in F12 was annealed to the fork. Given the self-complementarity with the fork position, the annealing can lead to the structure shown in Figure 3A. If the fork is in state S1, the new ssDNA will form a three-way junction with F12. However, if the fork is in state S2, a four-way Holliday junction will be formed instead.

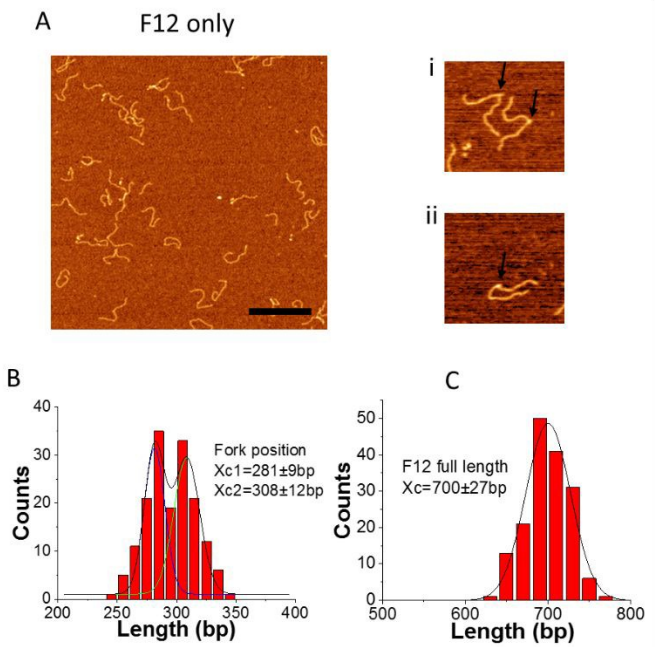

Figure 2. AFM analysis of the fork position for F12 (kinked DNA molecules). (A) Typical AFM images of fork DNA. The bar size is 300nm. Zoomed images (300nm x 300nm) of selected molecules with a clear appearance of the kinks (indicated with arrows) are shown to the right (i and ii). (B) and (C) are the distributions of fork positions measured from the parental dsDNA end and the full length of F12, respectively. The distributions were fitted by Gaussians and the fitting values Xc which is defined by the maxima values ± SD are indicated on the histograms.

The representative AFM images of the annealed DNA are shown in Figure 3B. The enlarged pictures are two types of DNA corresponding to different Holliday junctions (indicated with arrows). We performed mapping of the fork position and those data are shown in Figure 3C. The distribution was fitted with two Gaussians. The averaged position of two peaks is 283 ± 6bp and 309 ± 11bp, which are the same as the two peaks measured by the kink position on free DNA (Figure 2B). The distribution of full length of F12 was fitted with single peak Gaussian, and the average length is 700 ± 26bp as shown in Figure 3D. These data suggest that the fork with the annealed ssDNA complement undergoes dynamics between the 3-way and 4-way geometries. This dynamic of the junction was visualized directly with HS-AFM (Supplementary movie S1 and selected frames in Fig. S2A).

Open Access Article. Published on 11 February 2020. Downloaded on 2/21/2020 10:39:26 AM.
This article is licensed under a Creative Commons Attribution 3.0 Unported Licence.

Nanoscale Advances Accepted Manuscript

View Article Online
DOI: 10.1039/C9NA00712A

This dataset demonstrates that initially highly dynamic three-way junction adopts four-way junction geometry. In selected frames in Supplementary Figure S2A, Images 1 and 2 correspond to the three-way geometry of the fork, whereas images 3 and 4 show the four-way junction geometry; this conformational transition is illustrated schematically in supplementary Figure S2B. Additionally, we measured positions of junctions from the DNA ends (parental DNA strands) and these values are 286 ± 4 bp for three-way junctions (1, 2) and 313 ± 2 bp for four-way junctions (3, 4).

We also annealed the same extra 69 ssDNA to F4 even though the complementary region is only 28 nt on F4. The annealed double strand is still visible as shown in Supplementary Figure S3A. The position was measured and shown in Supplementary Figure S3B. The average value is still 271 ± 16 bp as expected for the designed fork position.

The binding of SSB to F12 fork does not affect fork dynamics.

To ensure that F12 could be used for fork regression analyses, it was first necessary to determine whether SSB affected the equilibrium between states 1 and 2. Therefore, we imaged SSB bound to F12 in the absence of ATP, to mimic fork regression buffer conditions. Typical AFM images of SSB-F12 complexes (indicated with arrows) in the absence of ATP in the binding buffer are shown in Figure 4A.

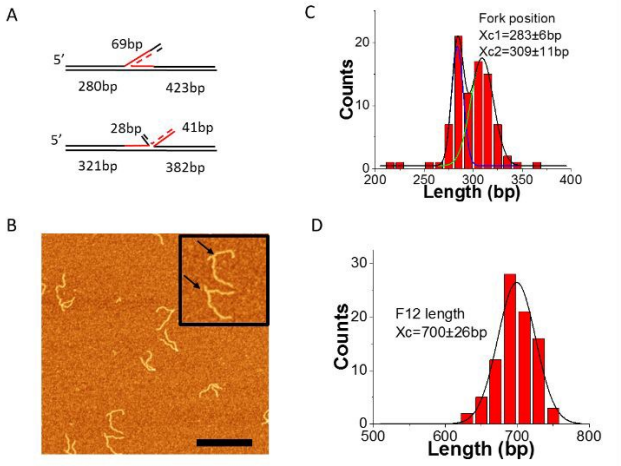

Figure 3. AFM analysis of the fork position on F12 probed by annealing with a complementary 69 nt ssDNA. (A) The scheme of new ssDNA annealed with the two states of F12. (B) AFM images of annealed fork DNA with 69nt ssDNA on APS mica. The bar size is 300nm. Insets show the enlarged images of fork DNA with annealed double strand fragment (indicated with arrows) at fork (300nm x 300nm). (C) and (D) are distribution of fork positions measured from the end of the short DNA flank and the full length of F12, respectively. Gaussian fits for the length distributions by double peak (C) and a single peak Gaussians (D); the maxima values ± SD are indicated on the histograms.

SSB appears as a bright feature. The location of the protein on the fork was measured from the end of the parental strand, and the distribution of SSB positions are shown in Figure 4B. The distribution is broad and can be fitted with two Gaussians. The average SSB positions are 285 ± 18 bp and 317 ± 13 bp which

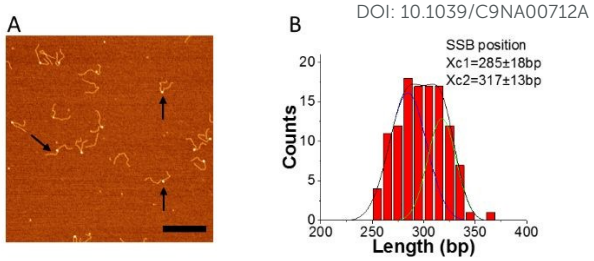

Figure 4. SSB binding does not alter the S1 to S2 equilibrium. (A) representative image of SSB bound to F12 in the absence of ATP (arrows pointed to some typical complexes of SSB with F12). The bar size is 300nm. (B) is the distribution of SSB positions obtained from images such as those shown in panel A. The distribution was fitted by double peak Gaussians and the maxima values ± SD was indicated on the histograms.

correlate with the fork position on free DNA (Figures 1 and 2). This result suggests that SSB binds to the fork in both states and does not affect the migration of the joint fork. The dynamic of SSB on single F12 was also monitored with time-lapse AFM and displayed in Supplementary movie S2 (one out of five movies analyzed). The scanning time for each frame is 30s. The mapping results for SSB on F12 for each frame is showed in Supplementary Figure S4A. In the mapping, the DNA was aligned to the end of short duplex region. The histogram of SSB position is shown in the supplementary figure S4B. The histogram is well approximated by a single peak Gaussian which suggests that once bound to the DNA, SSB does not slide.

RecG regresses F12 to state S2 in presence of ATP.

Next, we performed experiments in which both SSB and RecG were bound to the same DNA substrate. In these experiments, SSB and RecG were premixed and then F12 was added and the experiments were performed in the absence and presence of ATP. Typical AFM images are shown in Figure 5A and C.

Most of the DNA-protein complexes appear as particle assemblies along with a few double-particle complexes in which one particle is larger than the other one. The volume of the complexes (single particles and the larger one in double particles indicated with arrows), in Figure 5A was measured and distribution is shown in Supplementary Figure S5. The histogram was fitted with a Gaussian, and the average volume is 155.8 ± 30 nm^3 which is close to the volume of SSB (122.8 ± 22 nm^3) [14]. This suggests that the single protein or the larger protein in the double particles is SSB, while the smaller "blob" corresponds to RecG consistent with our previous work [14].

Open Access Article. Published on 11 February 2020. Downloaded on 2/21/2020 10:39:26 AM.
This article is licensed under a Creative Commons Attribution 3.0 Unported Licence.

Nanoscale Advances Accepted Manuscript

This journal is © The Royal Society of Chemistry 20xx

View Article Online
DOI: 10.1039/C9NA00713A

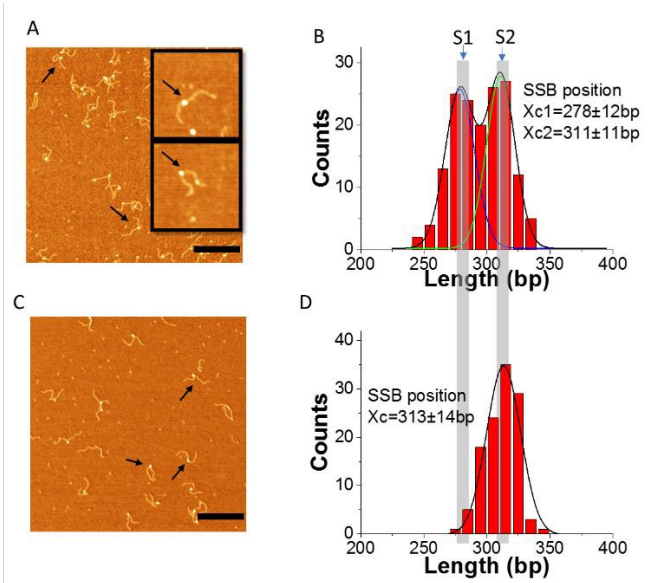

Figure 5. RecG migrates the fork in an ATP hydrolysis-dependent manner. (A) and (C), representative images of complexes of F12 mixed with SSB and RecG. A, absence of ATP; C, presence of ATP in the binding buffer. The bar size is 300nm. The two insets in (A) show the typical single and double particles on DNA (300nm x 300nm) (arrows pointed to some typical complexes of SSB with F12). (B) and (D) are the distribution of SSB position obtained from panels (A) and (C), respectively. The histograms are fitted with double and single peak Gaussians and the maxima values ± SD are indicated on the histograms.

To check if RecG can change the binding of SSB to F12, we measured the position of SSB on F12, and the histograms are displayed in Figure 5B and D. In the absence of ATP, the distribution of SSB is still broad and can be fitted with two peak Gaussians. The peak values are 278 ± 12 bp and 311 ± 11 bp, which are similar to the distribution observed in the complexes of SSB only with DNA. In contrast, when the buffer contains ATP, the distribution of SSB positions is narrow and can be fitted with a single peak Gaussian. The average position is 313 ± 14 bp which corresponds to state S2 of F12. These results suggest that when RecG is active in the presence of ATP, it can rewind the complementary region on the fork substrate displacing SSB from the ssDNA.

To investigate if the shift in the position of SSB was due to the regression of DNA by RecG, we performed experiments in the presence of the non-hydrolysable analog ATPγS, instead of ATP. First, the position of SSB alone in the presence of ATPγS was determined and is shown in Supplementary Figure S6. The histogram was fitted with a two-peak Gaussian. The average positions are at 289 ± 7bp and 313 ± 8bp, which are very close to positions of SSB in the absence of ATP. As a control, to determine whether ATP can change the binding activity of SSB to F12, the complex of SSB-F12 in the presence of ATP was made, and SSB positions determined (Supplementary Figure S7). The fitting of the histogram shows also two peaks of SSB positions on F12, and the averages are 290 ± 16bp and 316 ± 7bp. The distribution of SSB position on F12 is the same in the presence and absence of ATP or ATPγS in the binding buffer. This result suggests that ATP does not affect the position of SSB on F12.

Similar experiments were done for RecG to determine whether fork position is altered in the presence of nucleoside triphosphate (Supplementary Figure S8). In the absence of ATP, the RecG position on F12 can be fitted with a single peak, and the position 281 ± 16bp corresponds to state S1 of F12 (Supplementary Figure S8A). In the presence of ATP, the distribution of RecG is broad and can be fitted with two Gaussians. The peak positions are 280 ± 15bp and 310 ± 16bp. The new maximum at 310 bp suggests that RecG binds to the fork and regresses it from state S1 to state S2. The results suggest that, in the absence of ATP, RecG state S1 which mimics an ssDNA gap on the leading strand consistent with previous work [5]. In contrast, in the presence of ATP, RecG catalyzes the regression of the fork from state S1 to S2. However, due to the design of the fork, a fraction of the regressed forks revert back to S1 once RecG disengages from the DNA.

RecG binding to F12 fork in presence of SSB and ATP.

To characterize coupling of RecG catalyzed fork regression and the interaction with SSB, additional analysis was performed. Consequently, positions of SSB and RecG on the fork in the complexes containing both proteins were measured as well as the yield of each complex. Figure 6A presents the results of F12 mixed with SSB or RecG only. The yields of SSB-F12 complexes (blue columns) were similar to each other in the absence (left) and the presence (right) of ATP in the buffer. When F12 was mixed with both SSB and RecG, the yield of RecG-F12 complexes was counted by the complexes which contained double particles on the same DNA (similar to the methods with F4 [13, 14]). The yield of SSB-F12 complexes was obtained by counting all the complexes including single or double particles. The yield of complexes of SSB only with F12 (Figure 6A) is identical to the overall yield of complexes in the mixture of SSB and RecG together with F12 (Figure 6B). Similarly, the yield of complexes of RecG only with F12 (Figure 6A) is identical to the yield of double-particle complexes in the mixture of SSB and RecG together with F12 (Figure 6B). Note that the presence of SSB did not increase the binding of RecG to the fork substrate which is different from our previous data using a static fork F4 in which the SSB mediated remodeling of RecG was the major factor defining the elevated yield of RecG complexes with DNA [14]. This finding suggests that the dynamics of F12 fork between states S1 and S2 is the factor contributing to the RecG remodeling process.

Open Access Article. Published on 11 February 2020. Downloaded on 2/21/2020 10:39:26 AM.
This article is licensed under a Creative Commons Attribution 3.0 Unported Licence.

Nanoscale Advances Accepted Manuscript

View Article Online
DOI: 10.1039/C9NA00734A

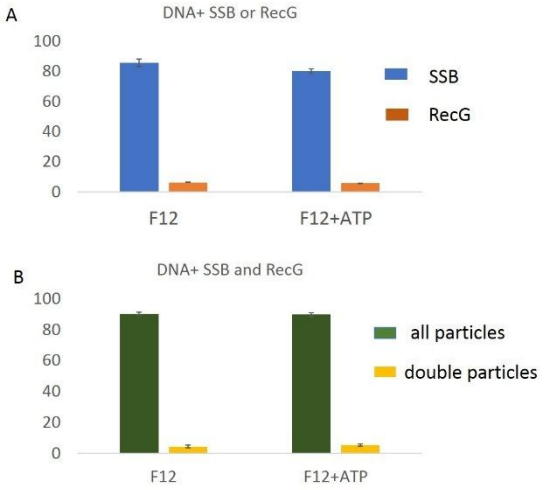

Figure 6. The yield of complexes for different DNA protein mixtures. (A) The columns show the yield of F12 with SSB (blue) or RecG (orange) when DNA was mixed with only one protein without and with ATP in the buffer. (B) The columns show the yield of SSB (all particles) and RecG (double particles) when DNA was mixed with SSB and RecG without and with ATP in the buffer.

We also analyzed maps of complexes containing both SSB and RecG (Supplementary Figures S9 and S10) which can be distinguished by different sizes on AFM images. The maps show that SSB (larger blobs) and RecG (smaller blobs) localize to different places on F12 DNA. We measured the position of both SSB and RecG on DNA as well as the arm length of F12 on both sides of SSB. The mapping of SSB and RecG on F12 is shown in Supplementary Figure S9B and S10B. In the mapping, the DNA was aligned to the position of SSB. RecG was observed to localize to both sides of SSB suggesting that RecG translocates on F12. The distance between SSB and RecG was measured and the data are shown in Supplementary Figures S9C and S10C. SSB position was assigned to "0" in these maps. When RecG was on the parental strand, the value of distance is negative, and when RecG is on the nascent strand, the value is positive. Analysis shows that the histograms of the SSB-RecG distance are similar in the absence and presence of ATP. RecG position appears broadly on F12 and is expected for an active process on a dynamic fork. As we reported earlier[13], RecG translocates to the side of SSB in both direction in an ATP independent manner. This is another difference between the two types of forks pointing to the role of the dynamics of the fork in the assembly of RecG with the fork [13].

Discussion

The primary conclusion of this AFM study is that RecG drives fork regression and in the process, displaces SSB from the DNA. The AFM results are consistent with previous single-molecule studies with magnetic tweezers [5, 19]. By using a static fork substrate in the previous study, we demonstrated that SSB facilitates the loading of RecG onto the fork and in the process, remodels the helicase [14]. Remodeling involves binding of the linker domain of SSB to the OB-fold of RecG so that fork binding is precluded [20-22]. Consequently, RecG, with binding predicted to be mediated by the helicase domains, binds preferentially to the parental duplex region ahead of the fork. Importantly, in this remodeled state, RecG is capable of spontaneous migration over the DNA duplex, and we hypothesized that in this new role RecG checks the DNA duplex integrity [13]. In fact, mismatches in this region impair RecG binding onto the parental DNA duplex (manuscript in preparation).

As a static fork was used in the previous study, it was not possible to study the fork regression reaction catalyzed by this enzyme. Therefore, a mobile fork design was required, designated F12. This fork substrate equilibrates between two states: S1, corresponding to a stalled fork and S2, corresponding to a regressed fork. Results show that both states formed with equal probability and that SSB bound to each state without a clear preference (Figures 2, 3 and 4B). The HS-AFM data (Supplementary Figure 2) directly visualize the transition of F12 fork complexed with ssDNA complement DNA between states S1 and S2.

Binding of RecG to F12 DNA remains transient, so that complex yield remains as low as 6.3% and is unaffected by the presence of ATP. Furthermore, the presence of ATP does not change the partition of F12 DNA between states S1 and S2 (Supplementary Figure S8B). This follows because any action by RecG would result in the transition from state S1 to S2 due to the ability of the helicase to regress the fork. However, a fraction of the regressed fork will revert back to S1, thereby reestablishing the equilibrium. In contrast, when SSB is present in the regression reaction, it binds to the product S2, trapping the fork and producing an increase in the ratio of S2:S1. The RecG-dependent shift in this ratio was only observed in the presence of ATP since the equilibrium between S1 and S2 was unaltered in the absence of ATP or in the presence of the non-hydrolyzable analog, ATPγS. Control experiments demonstrate that SSB alone does not alter the S1:S2 ratio and it can maintain the status of the fork state after binding to F12. Therefore, the only way this ratio could be altered is if RecG bound to the SSB-DNA complex and then used ATP binding and hydrolysis to drive fork regression, concomitant with SSB displacement.

Similar to previous studies with the static F4 fork [14], we were able to observe SSB mediated remodeling of RecG by direct visualization of complexes of F12 in which the two proteins were bound. We termed these "two-blob complexes" (Figure 5 and Supplementary Figure S9A). In these complexes, SSB position coincides with the location of the fork, whereas RecG binds to DNA far from the fork. Note that both proteins appear on the AFM images as globular features of different sizes with SSB being larger than RecG, allowing the discernment of protein identity as shown previously [13, 14]. We mapped RecG position using SSB as a marker (Supplementary Figure S9B) and the data have shown that remodeled RecG binds to both DNA duplexes with almost the same affinity. Thus, regardless of whether the fork is static or dynamic, SSB-loading of RecG concomitant with helicase remodeling is observed. This suggests that remodeling is intrinsic to the SSB-mediated loading process.

Open Access Article. Published on 11 February 2020. Downloaded on 2/21/2020 10:39:26 AM.
This article is licensed under a Creative Commons Attribution 3.0 Unported Licence.

Nanoscale Advances Accepted Manuscript

This journal is © The Royal Society of Chemistry 20xx

Although the remodeling of RecG by SSB was observed on the dynamic fork, the yield of double-blob complexes was considerably lower when compared with the static fork used previously [14]. This finding suggests that once loaded onto the parental duplex, RecG slides back to the fork, the wedge domain engages the fork, resulting in regression and displacement of SSB and this dynamics is coupled to ATP hydrolysis. For this to occur, SSB must slide some short distance on the ssDNA tail and away from the fork to permit wedge domain access. SSB sliding has been demonstrated [23]. In contrast, RecG sliding prior to the onset of regression can only occur when the duplex DNA is undamaged. Ultimately this ensures that regression does not occur and other repair enzymes must process the DNA first.

Conclusions

In this study, we demonstrated that the interaction of SSB and RecG with the mobile fork DNA. We found that the mobile fork migrated simultaneously between two different states. The presence of SSB did not change but stabilized the two states of the fork structure. ATP did not affect the interaction of SSB with fork DNA. RecG in the presence of SSB had two different modes of interaction with fork DNA. In first mode, RecG was remodeled by SSB and translocated along the duplex region. In second mode, in the presence of ATP, RecG's helicase activity was active and regressed the fork in an ATP-dependent manner. The regression of RecG displaced the SSB on the ssDNA at the fork.

Conflicts of interest

There are no conflicts to declare.

Acknowledgements

The work was supported by the National Institutes of Health grants R01 GM118006 to YLL and R01 GM100156 to PRB and YLL.

Notes and references

1 T. Kogoma, *Microbiology and molecular biology reviews : MMBR*, 1997, **61**, 212-238.
2 A. Kuzminov, *Microbiology and molecular biology reviews : MMBR*, 1999, **63**, 751-813, table of contents.
3 S. C. Kowalczykowski, *Trends in biochemical sciences*, 2000, **25**, 156-165.
4 P. Sung and H. Klein, *Nature Reviews Molecular Cell Biology*, 2006, **7**, 739-750.
5 M. Manosas, S. K. Perumal, P. R. Bianco, F. Ritort, S. J. Benkovic and V. Croquette, *Nature communications*, 2013, **4**, 2368.
6 S. L. Slocum, J. A. Buss, Y. Kimura and P. R. Bianco, *Journal of molecular biology*, 2007, **367**, 647-664.
7 J. A. Buss, Y. Kimura and P. R. Bianco, *Nucleic Acids Res*, 2008, **36**, 7029-7042.
8 M. R. Singleton, S. Scaife and D. B. Wigley, *Cell*, 2001, **107**, 79-89.
9 A. A. Mahdi, G. S. Briggs, G. J. Sharples, Q. Wen and R. G. Lloyd, *The EMBO journal*, 2003, **22**, 724-734.
10 S. Abd Wahab, M. Choi and P. R. Bianco, *J Biol Chem*, 2013, **288**, 26397-26409.
11 D. Hargreaves, J. B. Rafferty, S. E. Sedelnikova, R. G. Lloyd and D. W. Rice, *Acta crystallographica. Section D, Biological crystallography*, 1999, **55**, 263-265.
12 T. A. Windgassen, M. Leroux, S. J. Sandler and J. L. Keck, *The Journal of biological chemistry*, 2019, **294**, 2801-2814.
13 Z. Sun, M. Hashemi, G. Warren, P. R. Bianco and Y. L. Lyubchenko, *Biochemistry*, 2018, **57**, 1967-1976.
14 Z. Sun, H. Y. Tan, P. R. Bianco and Y. L. Lyubchenko, *Sci Rep*, 2015, **5**, 9625.
15 S. C. Gill and P. H. von Hippel, *Analytical biochemistry*, 1989, **182**, 319-326.
16 T. M. Lohman, J. M. Green and R. S. Beyer, *Biochemistry*, 1986, **25**, 21-25.
17 J. Liu, M. Choi, A. G. Stanenas, A. K. Byrd, K. D. Raney, C. Cohan and P. R. Bianco, *Protein science : a publication of the Protein Society*, 2011, **20**, 1005-1020.
18 T. M. Lohman and L. B. Overman, *The Journal of biological chemistry*, 1985, **260**, 3594-3603.
19 H. Y. Tan, L. A. Wilczek, S. Pottinger, M. Manosas, C. Yu, T. Nguyenduc and P. R. Bianco, *Protein Sci*, 2017, **26**, 700-717.
20 P. R. Bianco, S. Pottinger, H. Y. Tan, T. Nguyenduc, K. Rex and U. Varshney, *Protein Sci*, 2017, **26**, 227-241.
21 P. R. Bianco and Y. L. Lyubchenko, *Protein Sci*, 2017, **26**, 638-649.
22 P. R. Bianco, *Progress in biophysics and molecular biology*, 2017, **127**, 111-118.
23 R. Zhou, A. G. Kozlov, R. Roy, J. Zhang, S. Korolev, T. M. Lohman and T. Ha, *Cell*, 2011, **146**, 222-232.

View Article Online
DOI: 10.1039/C9NA00712A

Open Access Article. Published on 11 February 2020. Downloaded on 2/21/2020 10:39:26 AM.
This article is licensed under a Creative Commons Attribution 3.0 Unported Licence.

Nanoscale Advances Accepted Manuscript